HHS Public Access

Author manuscript

J Comp Neurol. Author manuscript; available in PMC 2018 December 01.

Published in final edited form as:

J Comp Neurol. 2017 December 01; 525(17): 3653–3665. doi:10.1002/cne.24293.

Melanopsin ganglion cell outer retinal dendrites: Morphologically distinct and asymmetrically distributed in the mouse retina

Katelyn B. Sondereker[1], **Jessica R. Onyak**[1], **Shakib W. Islam**[1], **Christopher L. Ross**[1], and **Jordan M. Renna**[1,*]

[1]Department of Biology, The University of Akron, Akron, Ohio, USA

Abstract

A small population of retinal ganglion cells express the photopigment melanopsin and function as autonomous photoreceptors. They encode global luminance levels critical for light-mediated non-image forming visual processes including circadian rhythms and the pupillary light reflex. There are five melanopsin ganglion cell subtypes (M1–M5). M1 and displaced M1 (M1d) cells have dendrites that ramify within the outermost layer of the inner plexiform layer (IPL). It was recently discovered that some melanopsin ganglion cells extend dendrites into the outer retina. Outer Retinal Dendrites (ORDs) either ramify within the outer plexiform layer (OPL) or the inner nuclear layer (INL), and while present in the mature retina, are most abundant postnatally. Anatomical evidence for synaptic transmission between cone photoreceptor terminals and ORDs suggests a novel photoreceptor to ganglion cell connection in the mammalian retina. While it is known that the number of ORDs in the retina is developmentally regulated, little is known about the morphology, the cells from which they originate, or their spatial distribution throughout the retina. We analyzed the morphology of melanopsin-immunopositive ORDs in the OPL at different developmental time points in the mouse retina and identified five types of ORD originating from either M1 or M1d cells. However, a pattern emerges within these: ORDs from M1d cells are generally longer and more highly branched than ORDs from conventional M1 cells. Additionally, we found ORDs asymmetrically distributed to the dorsal retina. This morphological analysis provides the first step in identifying a potential role for biplexiform melanopsin ganglion cell ORDs.

*Corresponding Author: Jordan M. Renna, Ph.D., Department of Biology, University of Akron, Akron, OH 44325-3908, Office: 330-972-6933, Fax: 330-972-8445, jrenna@uakron.edu.

CONFLICT OF INTEREST STATEMENT

There is no conflict of interest to report.

ROLE OF AUTHORS

All authors had full access to all the data in the study and take responsibility for the integrity of the data and the accuracy of the data analysis. Study concept and design: KBS, JMR. Acquisition of data: KBS, JLO, SWI. Analysis and interpretation of data: KBS, JLO, SWI, CLR, JMR. Drafting of the manuscript: KBS, JLO, JMR. Critical revision of the manuscript for important intellectual content: KBS, JMR. Statistical analysis: KBS. Obtained funding: JMR. Administrative, technical, and material support: JMR. Study supervision: JMR.

Keywords

melanopsin; ipRGCs; biplexiform; outer retinal dendrite; photoreceptor; retina; RRID: AB_2314781; RRID: AB_2301751; RRID: AB_2629482; RRID: AB_2158332

INTRODUCTION

In the mature mammalian retina, a small population of retinal ganglion cell output neurons express the photopigment melanopsin and function as autonomous photoreceptors (Provencio et al., 1998; Provencio et al., 2000; Berson et al., 2002; Hattar et al., 2002; Dacey et al., 2005). There are at least five known subtypes of these melanopsin ganglion cells (M1–M5) that differ in characteristics including soma size, retinal stratification, dendritic field size, level of melanopsin expression, and axonal projections (Hattar et al., 2002; Berson et al., 2010; Ecker et al., 2010; Schmidt and Kofuji, 2011; Estevez et al., 2012). M1 melanopsin ganglion cells predominantly innervate non-image forming brain targets including the superchiasmatic nucleus to mediate circadian photoentrainment, and the olivary pretectal nucleus for regulation of the pupillary light reflex (Hattar et al., 2002; Baver et al., 2008; Guler et al., 2008; Schmidt et al., 2011). M1 melanopsin ganglion cells have somas located in both the ganglion cell layer (GCL) and displaced (M1d) to the inner nuclear layer (INL). Both M1 and M1d cells have dendrites that stratify within the outermost plexus of the OFF sublamina in the inner plexiform layer (IPL), where they make *en passant* (in passing) contact with ON bipolar cell axons and synaptic contact with dopaminergic amacrine cells (Vugler et al., 2007; Zhang et al., 2008; Hoshi et al., 2009; Berson et al., 2010). However, during development, a subpopulation of melanopsin ganglion cells extend dendrites into both the IPL and to either the outer plexiform layer (OPL) or the inner nuclear layer (INL) (Renna et al., 2015). These dendrites have been termed Outer Retinal Dendrites (ORDs) and ORDs in the OPL closely associate with cone axon terminals (Renna et al., 2015). At postnatal day 4 (P4), ORDs are virtually nonexistent. As postnatal retinal development progresses, the number of ORDs stratifying within the OPL and INL increases, with the highest density occurring between P8 and P12. As the retina continues to mature, ORD density decreases.

ORDs that extend into the OPL ramify in close apposition to cone photoreceptor terminals, suggesting synaptic transmission between cone photoreceptors and melanopsin ganglion cell ORDs. Postsynaptic glutamate density protein 95 (PSD95), a marker for excitatory synapses, has been shown to be closely associated with ORDs in the OPL, suggesting that ORDs are the postsynaptic partner to glutamate-releasing cone photoreceptors (Renna et al., 2015). A cone to biplexiform ganglion cell circuit defies the conventional mammalian retinal signaling pathway in which bipolar cells function as an intermediate between photoreceptors and ganglion cells. This potentially novel circuit may have evolutionary significance, as photoreceptor to ganglion cell connections are the predominate retinal circuit in invertebrates such as the hagfish (Holmberg, 1970). In addition, ORDs have recently been seen in macaque retinal tissue (Liao et al., 2016), further suggesting that this potential ganglion cell-photoreceptor circuit has been evolutionarily conserved.

Anecdotal evidence suggests ORDs originate from M1 and M1d melanopsin ganglion cells (Renna et al., 2015). Although melanopsin ganglion cells are distributed evenly across the entire retina, M1 and M2 cells are predominantly located in the dorsal retina, while M4 and M5 cells are predominantly located in the ventral retina (Hughes et al., 2013; Valiente-Soriano et al., 2014). Interestingly, it has been postulated that there is a correlation between the dorsal and ventral asymmetrical distribution of both melanopsin ganglion cells and cone photoreceptor opsins. In the mouse retina, most cones co-express m-opsin (medium wavelength opsin) and s-opsin (short wavelength opsin). M-opsin is expressed at low concentrations in the ventral retina and high concentrations in the dorsal retina (Applebury et al., 2000). In contrast, s-opsin is predominantly expressed in the ventral retina (Applebury et al., 2000).

Despite anecdotal evidence suggesting ORDs originate from M1 and M1d cells, this has not yet been confirmed, nor has there been a comprehensive morphological analysis of ORDs. Here we provide a more complete description of ORDs in the OPL at different developmental stages of the mammalian retina and investigate the distribution of melanopsin ganglion cell ORDs across the entire retina in relation to s-opsin expression.

MATERIALS AND METHODS

Animals

All experiments were conducted according to NIH guidelines under protocols approved by the Institutional Animal Care and Use Committees of the University of Akron. Wild-type male and female C57BL/6N mice were used for all experiments and were housed in cages in the University of Akron vivarium. Mice were used at ages P8, P12, and P30 (adult). 24 mice (48 retinas) were used in total for this study. All animals were maintained on a 12-hour light: dark cycle.

Antibodies

The primary antibodies (Table 1) used in this study have been characterized in the mammalian retina, and our staining patterns match those documented in other studies.

The polyclonal anti-melanopsin antibody (Advanced Targeting Systems, Cat# AB-38 [UF006], RRID: AB_2314781) was raised in rabbit against 15 N-terminal amino acids (MDSPSGPRVLSSLTQC) of the mouse melanopsin protein. The specificity of this antibody for the mouse melanopsin protein has been demonstrated by Panda et al. (2002), in which the antibody reveals no reactivity in melanopsin knockout mice. Additionally, Berson et al. (2010) showed lack of reactivity when this antibody was preabsorbed with its immunogen. The melanopsin staining pattern in our study matches that of studies done by Berson et al. (2010).

The polyclonal anti-vesicular glutamate transporter 1 (VGLUT1) antibody (Millipore, Cat# AB5905, RRID: AB_2301751) was raised in guinea pig against a synthetic peptide from the rat VGLUT1 protein (GATHSTVQPPRPPPPVRDY) and selectively labels the terminals of photoreceptors and bipolar cells (Johnson et al., 2003). The antibody specificity is demonstrated by colocalization with a well-characterized VGLUT1 antibody from RH

Edwards (Bellocchio et al., 1998). The VGLUT1 staining pattern shown here is the same as the staining pattern in the mouse retina of previous studies (Bellocchio et al., 1998; Sherry et al., 2003; Phillips et al., 2010).

The polyclonal anti-s-opsin antibody (Santa Cruz Biotechnologies, Cat# sc14363, RRID: AB_2158332) was raised in goat against 20 N-terminal amino acids (EFYLFKNISSVGPWDGPQYH) of the human OPN1SW protein. The specificity of this antibody was demonstrated by lack of reactivity when preabsorbed with its immunogen (Schleich et al., 2010). This s-opsin antibody has previously been characterized in retinal studies and has been shown to reliably label s-opsin cone outer segments (Haverkamp et al., 2001; Schiviz et al., 2008).

Immunohistochemistry

In order to determine morphology of ORDs in the OPL, triple label immunohistochemistry staining of retinal wholemounts from C57BL/6N mice at postnatal days 8, 12, and 30 (adult) was conducted similarly to Renna et al. (2015). The eyes were dissected in 0.1M phosphate-buffered saline (PBS) immediately after euthanasia and the retinas were mounted on nitrocellulose membrane ganglion cell side up. Retinas were then fixed in phosphate-buffered paraformaldehyde (4%) for 45 minutes. After a wash (3 × 15 minutes in PBS), the retinas were placed in blocking solution (1.7% Triton-X and 5.2% donkey normal serum in PBS) at 4° C overnight. The retinas were then incubated and shaken on a rotator for 6 days at 4° C in blocking solution with a mixture of primary antibodies: rabbit anti-melanopsin (Advanced Targeting Systems, Cat# AB-38 [UF006], RRID: AB_2314781 at 1:10,000) and guinea pig anti-VGLUT1 (Millipore, Cat# AB5905, RRID: AB_2301751 at 1:1000) to assess proximity of melanopsin-immunopositive dendrites to cone pedicles. For determining asymmetric distribution of ORDs, the primary antibodies used were goat anti-s-opsin (Santa Cruz Biotechnology, Cat# sc14363, RRID: AB_2158332 at 1:500) and rabbit anti-melanopsin (Advanced Targeting Systems, Cat# AB-38 [UF006], RRID: AB_2314781 at 1:10,000). After the incubation period, the retinas were washed (6 × 10 minutes in PBS), incubated, and shaken on a rotator overnight at 4° C in blocking solution with a mixture of secondary antibodies: donkey anti-rabbit Alexa 594 (Life Technologies, Cat# A21207) at 1:200 for melanopsin and goat anti-guinea pig Alexa 488 (Life Technologies, Cat# A11073) at 1:200 for VGLUT1. Retinas used for determining asymmetric distribution of ORDs were incubated and shaken on a rotator overnight at 4° C in blocking solution with the secondary antibodies donkey anti-goat Alexa Fluor 594 (Life Technologies, Cat# A11058) to visualize the s-opsin gradient and donkey anti-rabbit Alexa Fluor 488 (Life Technologies, Cat# A21206) for melanopsin. Before the retinas were washed a final time (6 × 10 minutes in PBS), either DRAQ5 (Thermofisher Scientific, Cat# 62252) at 1:200 or DAPI (Invitrogen, Cat# D1306, RRID: AB_2629482) at 1:200 was added to the blocking solution and incubated for 30 minutes. The retinas were then mounted on a glass slide with ProLong Gold anti-fade reagent with DAPI (ThermoFisher Scientific, Cat# P36931) or Aquamount and covered with a 1.5 μm thick coverslip.

Image acquisition and quantification

Melanopsin-immunopositive dendrites in wholemount retinas were imaged using an Olympus FV1000 confocal laser-scanning microscope at 40x-oil or 60x-oil magnification and the images were acquired using Olympus FV1000 software. The z-stacks of confocal images were collected at 0.45 to 1.0 μm intervals and the images were analyzed using ImageJ software, version 1.49. Contrast and brightness of images were adjusted using ImageJ and Adobe Photoshop CS6. Additionally, noise was removed with the Despeckle function of ImageJ. Single optical sections were generated from a series of confocal images masked to correct for the imperfect flatness of the retina with Adobe Photoshop CS6.

The retinal stratification of melanopsin-positive dendrites was determined by comparing their location with the presence or absence of retinal cell bodies labeled with DRAQ5 or DAPI. VGLUT1, which labels cone photoreceptor terminals, was used as a secondary marker of OPL stratification. All quantification involving length and branch points of ORDs in this manuscript was done on ORDs that stratify in the OPL. Total dendritic length of melanopsin-immunopositive dendrites in the OPL was measured using Simple Neurite Tracer, an ImageJ plugin. The length of dendrite measured was only dendrite in the OPL, not the length that traverses the INL. If an ORD bifurcated once it reached the OPL, the measured length of the ORD included all branches of that dendrite. If the case occurred in which two ORDs originated separately from the soma (M1d) or separately from dendrites in the OFF sublamina of the IPL (M1 or M1d), these lengths were not added together but instead counted as separate ORDs. The number of branch points was counted for each ORD and soma size was measured as the longest distance across the cell body. To further characterize the morphology of cells with ORDs, construction of 2-D morphology tracing was completed for a selected set of cells (as seen in Figure 2) in Adobe Photoshop CS6, using the confocal z-stacks as a template. The pencil tool was used to trace the processes of melanopsin-immunopositive cells.

Determining the subtypes of cells that have ORDs

To definitively determine the subtype of melanopsin ganglion cells that have ORDs in the OPL, we analyzed melanopsin-immunopositive dendrites in wholemount retinal confocal z-stacks. The high resolution of the images, as well as the nuclear counterstain allowed for better identification of ORDs and tracking the dendrites from the OPL to the soma than previous methods by Renna et al. (2015). ORDs in the OPL were identified as melanopsin-immunopositive dendrites that travel up to stratify within the OPL. These dendrites were traced through the retina to the soma of origin, either in the ganglion cell layer for conventional melanopsin ganglion cells or in the INL for displaced melanopsin ganglion cells. To be certain which soma the ORDs originated from, we visually traced 89 ORDs in the OPL from the soma to the OPL in high resolution confocal z-stack images of individual ORDs in the OPL. The soma size and IPL aborization assisted in identifying the subtype of melanopsin ganglion cells that exhibit ORDs. This method provides a more complete and comprehensive analysis of which subtypes of melanopsin ganglion cells extend ORDs into the OPL.

In addition to confocal z-stacks of individual ORDs, we also used an epifluorescence Zeiss Axioplan 2 microscope to record the cell of origin for every ORD (in both the INL and OPL) in wholemount retinas (n=4 retinas at P8, P12, and P30) stained for s-opsin and melanopsin. This was done by systematically locating a melanopsin-positive ORD and visually tracing it back to its soma of origin. Both the location of the ORD and the location of the soma it originated from was manually recorded on a retinal map.

Identifying retinal distribution of ORDs

Before enucleation, a ventral burn was made on the cornea. Once the eye was removed, a ventral cut was made based on the location of the burn in order to mark the ventral location of the retina. After wholemount retinas were stained (n=7 at P8, n=11 at P12, n=8 at P30) melanopsin-positive ORDs in both the INL and OPL were identified using a Zeiss Axioplan 2 or Olympus BX51 epifluorescence light microscope and their location was manually recorded on a retinal map. The s-opsin protein is known to be expressed at a higher concentration in the ventral portion of the mouse retina (Applebury et al., 2000), so the s-opsin gradient and the ventral cut were used to identify the ventral location of the retina. To calculate the highest concentration of s-opsin, a program was written with C# to identify the brightest region of s-opsin staining. The s-opsin distribution was considered to be highest in the area of the retina where the pixel intensity values were the highest. A vector was drawn through the center of the ventral retina, through the optic nerve, and through the dorsal retina to delineate the nasal retina from the temporal retina. A perpendicular line was drawn across the retina to distinguish the dorsal retina from the ventral retina. ORDs were either classified as being dorsally or ventrally located based on their location in reference to the s-opsin gradient. The area of the wholemount retinas was calculated using ImageJ, and the areas were used to extrapolate the mm^2 ORD counts from Renna et al. (2015) (n=4; 10.8 mm^2 at P8, 11.9 mm^2 at P12, and 12.4 mm^2 at P30).

Statistical analysis

Statistical analysis was conducted to determine difference in length of ORDs in the OPL between M1 and M1d cells at all developmental time points using one-way ANOVA and Bonferroni multiple comparisons test. Number of branch points of ORDs in the OPL was compared between M1 and M1d cells using one-way ANOVA and student’s t-test. For comparing the number or ORDs present across development, one-way ANOVA and Tukey-Kramer multiple comparisons test were used. Statistical analysis comparing the origins of ORDs and number of ORD positive cells was done with one-way ANOVA and Bonferroni multiple comparisons test. To assess the asymmetric distribution of ORDs at each developmental age, one-way ANOVA and Bonferroni multiple comparisons test were used to compare the number of ORDs located in the ventral retina to the number of ORDs located in the dorsal retina.

RESULTS

ORDs in the OPL are in close apposition to cone photoreceptor terminals

As previously noted by Renna et al. (2015), the number of ORDs reaching the OPL changes throughout development. This led us to search for morphological differences of ORDs in the

OPL at different stages of development (Fig. 1a1–b4). As seen in Figure 1, ORDs stratify within the OPL (Fig. 1c1–c4) and are closely opposed to cone pedicles at all stages of development, including the adult (Fig. 1d1–d4). Additionally, some ORDs extend through the INL, stratify within the OPL near cone photoreceptors, and then begin a descent back to the OFF sublamina of the IPL (data not shown). Although the majority of ORDs stratify in close apposition to cone photoreceptors, a small fraction of ORDs run along the inner portion of the OPL, but do not ascend high enough into the OPL to contact the cone photoreceptors. However, this stratification pattern seems to be an exception to the rule.

ORDs originate exclusively from biplexiform M1 and M1d melanopsin ganglion cells

Anecdotal evidence suggested that ORDs originate from M1 cells, both conventional and displaced, and also possibly M3 cells (Renna et al., 2015). We traced 89 different ORDs in confocal z-stacks to the cell of origin at various postnatal developmental time points and found ORDs originating from only M1 and M1d melanopsin ganglion cells (Fig. 2a1–a5; n=5 retinas at P8, n=7 retinas at P12, and n=5 retinas at P30). We have termed these cells biplexiform melanopsin ganglion cells because they stratify in the two plexiform layers: the IPL (Fig. 2b1–c5) and the OPL (Fig. 2d1–e5). The cells in our study were identified as M1 and M1d subtypes based on their stratification in only the S1 plexus of the OFF sublamina of the IPL (Fig. 2b1–c5) because this stratification pattern is a delineating morphological characteristic of both M1 and M1d melanopsin ganglion cells, setting them apart from the other subtypes. Overall, the morphology of these two subtypes of melanopsin ganglion cells that have ORDs is consistent with the morphology of M1 and M1d cells (Fig. 2).

Five types of ORDs in the OPL

We found five general types of ORDs in the OPL based on the subtype of melanopsin ganglion cell they originate from and the outer retinal dendrite morphology. ORDs from M1 cells branch off from dendrites in the S1 layer of the IPL, traverse the INL, and then run horizontally along the OPL. ORDs from M1 cells can be either unbranched (Fig. 2a1) or branched (Fig. 2a2). In contrast, ORDs from M1d cells usually originate from the soma and extend through the INL to stratify upon reaching the OPL. However, ORDs from M1d cells can also originate from dendrites in the S1 plexus of the IPL. ORDs from M1d cells can be either unbranched (Fig. 2a3), branched (Fig. 2a4), or have ORDs in both the OPL and the INL (Fig. 2a5).

M1 and M1d ORDs in the OPL are morphologically distinct

A distinct pattern of dendrite morphology emerges upon comparing ORDs based on the melanopsin ganglion cell subtype from which they originate. We examined both the length and the number of branch points at postnatal days 8, 12, and 30 (adult) of ORDs in the OPL from M1 and M1d cells, and found them to be morphologically distinct at most developmental time points (Fig. 3a, 3b). ORDs in the OPL originating from M1d cells are longer (Table 2; Fig. 3a; length of ORDs in the OPL from M1 cells at P8 [n=8]: 42.27 ± 7.03 μm; at P12 [n=19]: 69.54 ± 9.97 μm; at P30 [n=9]: 84.81 ± 13.74 μm; length of ORDs in the OPL from M1d cells at P8 [n=12]: 119.98 ± 29.49 μm; at P12 [n=15]: 194.11 ± 36.89 μm; at P30 [n=21]: 202.69 ± 43.17 μm) and have more branch points (Table 3; Fig. 3b; branch points of ORDs in the OPL from M1 cells at P8 [n=8]: 0.25 ± 0.16; at P12 [n=19]: 0.74

± 0.24; at P30 [n=9]: no branch points; branch points of ORDs in the OPL from M1d cells at P8 [n=12]: 1.5 ± 0.51; at P12 [n=15]: 1.33 ± 0.32; at P30 [n=21]: 0.81 ± 0.29) than those that originate from M1 cells at all stages of development. This appears to be largely due to the unbranched nature of ORDs in the OPL from M1 cells, as they usually run along the OPL without bifurcating, resulting in a shorter total dendrite length within the OPL. Indeed, the longest ORDs (typically >200 μm) are those that have two or more branch points (Fig. 3c).

The number of ORDs peaks at P12

To reevaluate the ORD density estimates made by Renna et al. (2015), we counted the total number of ORDs in wholemount retinas (Fig. 4a). At P8, there are 73.28 ± 4.74 ORDs, (n=7), and the number of ORDs increases as development progresses with 97.91 ± 8.05 ORDs (n=11) at P12. A large number of ORDs at P8 and P12 extend into the INL or the OPL but do not stratify in either layer, and these were included in our wholemount counts. The majority of these short, unbranched dendrites that terminate in the INL mostly originate from M1 melanopsin ganglion cells (data not shown). At P30, most of the dendrites classified as this type of ORDs are no longer present, which is consistent with the fact that there are only 35.13 ± 4.58 ORDs per retina at this age (n=8). Therefore, our data suggest that the number of ORDs peaks during development, around P12.

ORDs originate from a subset of M1 and M1d melanopsin ganglion cells

Only a subpopulation of M1 and M1d cells are biplexiform; that is, not every M1 or M1d cell has ORDs stratifying within the OPL or INL. To investigate the proportion of M1 and M1d cells that have ORDs throughout development we counted the total number of ORDs in wholemount retinas and classified them as originating from either an M1 or an M1d melanopsin ganglion cell (Table 4; Fig. 4b). At P8, 10.4% (24.75 ± 4.42 cells; n=4) of M1 cells are ORD-positive, while at P12 there are the highest number of ORD-positive M1 cells with 15.3% (46 ± 5.78 cells; n=4). Predictably, P30 retinas have the fewest number with only 4.7% of ORD-positive M1 cells (12 ± 3.42; n=4; Fig. 4b). The number of M1d ORD-positive cells follows a similar trend with 34.6% ORD-positive M1d cells at P8 (19.75 ± 1.59 cells; n=4), 28.3% ORD-positive M1d cells (19.25 ± 2.29 cells; n=4) at P12, and a reduction to 20.9% (14 ± 2.97 cells; n=4) of ORD-positive M1d cells at P30 (Fig. 4b). These cell counts follow a logical trend when considering how many ORDs are present in the retinas at each age. There are a larger number of ORD-positive cells during development, consistent with a larger number of ORDs during development. Most cells only have one ORD that reaches the OPL, but occasionally we found two or three ORDs originating from the same cell.

We then wanted to determine the composition of the population of ORDs based on whether they originate from M1 melanopsin ganglion cells or M1d melanopsin ganglion cells (Fig. 4c). Our data indicate that early in development (P8 and P12) the majority of ORDs in the population are from conventional M1 cells (61.57 ± 7.67% at P8 [n=4] and 68.16 ± 5.35% at P12 [n=4]). However, at P30 the ORD composition is the opposite, with the majority of ORDs in the population from M1d cells (63.69 ± 1.87%; n=4).

ORDs are asymmetrically distributed to the dorsal retina

M1 and M1d melanopsin ganglion cells are asymmetrically distributed to the dorsal retina (Hughes et al., 2013). Additionally, s-cone opsins are expressed in high concentrations in the ventral retina and low concentrations in the dorsal retina (Applebury et al., 2000; Szel et al., 2000). We therefore hypothesized that ORDs in the OPL and INL from M1 and M1d melanopsin ganglion cells would be asymmetrically distributed to the dorsal retina, where s-opsin expression is low. When ORDs are mapped onto a retina stained with s-opsin, the ORD distribution is heavy in the dorsal retina, opposite the s-opsin gradient (Fig. 5a–c). In the dorsal retina, there were 51.86 ± 4.27 ORDs at P8 (n=7), 72.90 ± 6.24 ORDs at P12 (n=11), and 27.75 ± 5.06 ORDs at P30 (n=8). In the ventral retina, there were 21.42 ± 3.47 ORDs at P8 (n=7), 25 ± 2.56 ORDs at P12 (n=11), and 7.25 ± 1.66 ORDs at P30 (n=8). Thus, at all developmental time-points, there were significantly more ORDs present in the dorsal retina than in the ventral retina (Fig. 5d). In contrast, ORDs are evenly distributed across the nasal and temporal retina (Fig. 5e). Additionally, the proportion of ORDs in the dorsal retina compared to the proportion of ORDs in the ventral retina remains constant across development (Fig. 5f). From our data, it appears ORDs are asymmetrically distributed to the dorsal retina, where m-opsin cones are in highest concentration.

DISCUSSION

A subset of M1 and M1d melanopsin ganglion cells are biplexiform with dendrites ramifying both in the IPL and either in the INL or the OPL. We have found five types of ORDs in the OPL categorized by their morphology and the melanopsin ganglion cell subtype from which they originate (Fig. 6). ORDs from M1 cells are either branched or unbranched, and originate from the dendrites in the S1 plexus. ORDs from M1d cells are branched or unbranched, and originate either from the dendrites in the S1 plexus or directly from the soma. The final type of ORD occurs only on M1d cells, in which multiple ORDs come from the same M1d cell, with some ORDs stratifying in the INL and others stratifying in the OPL. While these general types of morphologies exist, a pattern emerges when comparing M1 ORDs with M1d ORDs. Across development, ORDs originating from M1d melanopsin ganglion cells are longer and more highly branched than ORDs from M1 cells.

M1 and M1d cells are asymmetrically distributed to the dorsal retina (Hughes et al., 2013). Since ORDs originate exclusively from M1 and M1d cells, it is not surprising that we found them to be asymmetrically distributed to the dorsal retina as well. Early in development there is an initial increase in ORDs and as the retina matures the number of ORDs decreases. This increase in the number of ORDs is largely restricted to the dorsal retina. Specifically, the number of ORDs in the dorsal retina increases significantly from P8 to P12, while the number of ORDs in the ventral retina does not, indicating that the increase in total ORDs that occurs from P8 to P12 is due to an increase in dorsal ORDs. However, from P12 to P30, there is a significant decrease in dorsal ORDs as well as ventral ORDs, suggesting that the decrease in total ORDs that occurs from P12 to P30 is due to a decrease in ORDs from both the ventral and dorsal retina. This apparent difference in the development and subsequent pruning of ORDs suggests that ORDs in the dorsal retina are increasing during development, possibly reaching up to the dorsal OPL in search of a presynaptic partner, and then as the

retina matures, are pruned in both the dorsal and ventral retina at the same rate. Indeed, the morphological differences between M1 and M1d ORDs in the OPL of the mature retina, coupled with the morphological changes that occur within each subtype throughout development suggest ORDs are interacting with their environment as the retina matures.

Using small regions of interest, Renna et al. (2015) found 25.2 ± 5.5 ORDs per mm^2 at P8, 21.4 ± 4.7 ORDs per mm^2 at P12, and 5.6 ± 2.3 ORDs per mm^2 at P30, with no statistically significant difference between P8 and P12. Extrapolating out these numbers across the entire retina, they estimated approximately 272.3 ORDs per retina at P8, 255.1 ORDs at P12 and 75.2 ORDs at P30. Rather than estimating, we counted every ORD in each wholemount retina and found 73.3 ORDs at P8. The number or ORDs peaked at P12 (97.9 ORDs) and then decreased significantly by P30 as only 35.1 ORDs remained. It is possible that our numbers differ from those of Renna et al. (2015) because of the asymmetric distribution of ORDs in the retina. If their estimations were based on ORDs in an area of the retina that was more dense (such as the dorsal retina) or less dense (such as the ventral retina), the estimates would be skewed. Regardless, there are a larger number of ORDs early in development and a significant decrease in ORDs in the adult retina.

The total number of ORD-positive cells changes over development, with the most ORD-positive M1 cells at P12 and the most ORD-positive M1d cells at P8. This is consistent with our counts of total number of ORDs across development: As the number of ORD-positive cells decreases, so does the number of ORDs in the retina. The composition of ORDs in regards to the cell type they originate from also changes as development progresses. Though the total number of ORDs decreases throughout development, the proportion of ORDs arising from M1d cells increases as the retina matures, suggesting that the decrease in ORDs is largely due to a loss of ORDs arising from M1 cells. This change in composition of ORDs is not due to an increase in ORD-positive M1d cells, as it was stated above that there is a significant decrease in the number of ORD-positive M1d cells from P8 to P30. Rather, the shift in ORD composition is due to the significant decrease in ORD-positive M1 cells from P12 to P30, creating a situation in which the majority of ORDs that remain are from ORD-positive M1d cells. Thus, we can infer that the decrease in the number of ORDs to be largely due to elimination of the ORDs from M1 cells.

It appears that two specific types of ORDs may be reduced in number in the mature retina. We have anecdotally noted that there is a high number of ORDs at P8 and P12 that originate from M1 cells and extend straight up from dendrites in the S1 plexus and terminate in either the INL or OPL, without stratifying in either layer. Because these dendrites seem to originate from M1 cells and are almost completely gone by P30, it is plausible that the significant decrease in both ORD-positive M1 cells and ORDs from M1 cells is at least in part due to the loss of these ORDs as development progresses. Whether these ORDs retract or are pruned is not certain, but it appears their disappearance may be, as least in part, responsible for the change in ORD composition at P30. Additionally, a small percentage of ORDs in the OPL originating from conventional M1 ganglion cells branch early in postnatal development, but these branched ORDs appear to be lost in the mature retina. M1 ORDs in the OPL have a longer vertical distance to travel compared to M1d ORDs in the OPL.

Perhaps their arrival in the OPL does not coincide with the developmental cues required for ORDs to extend, branch and mature within the OPL.

While it is clear that ORDs are abundant early in development and less so in the mature retina, the functional role these dendrites play in the visual system remains unknown. The asymmetric distribution of ORDs to the dorsal retina, the area of the mouse retina with the highest density of m-opsin expression (Applebury et al., 2000; Szel et al., 2000), suggests some interaction with photoreceptors expressing this photopigment. Perhaps ORDs are postsynaptic to m-opsin expressing cones, as Renna et al. (2015) found postsynaptic density marker 95 labeling on ORDs in the OPL. This would defy conventional mammalian retinal circuitry where bipolar cells function as an intermediate between photoreceptors and ganglion cells, and would be the first example of an outer retinal photoreceptor directly coupled to a ganglion cell. Because ORDs in the OPL are present in highest number during development and ramify in close apposition to cone photoreceptor terminals, ORDs may have a role in the development and distribution of cone opsins in the mouse retina.

At the same time that ORDs are extending into the OPL (P4–P12), waves of activity sweep across the inner retina and drive melanopsin ganglion cells to depolarize (Renna et al., 2011). Melanopsin is the first functional photopigment in development (Fahrenkrug et al., 2004; Sekaran et al., 2005; Schmidt et al., 2008), and light-mediated melanopsin ganglion cell signaling modulates conventional ganglion cells spiking during retinal wave activity (Renna et al., 2011; Kirkby and Feller, 2013). This suggests melanopsin ganglion cells can feed signals back into the inner retina. In the absence of light, melanopsin ganglion cells are depolarized by retinal wave activity and are critical for visual system development. When 200 M1 ganglion cells are deleted, both image forming and non-image forming systems fail to mature properly (Chew et al., 2017). ORDs may provide a medium for either retinal wave activity in the inner retina, or light-mediated melanopsin ganglion cell signaling from the inner retina to reach the outer retina, making ORDs a candidate for outer retinal development to be influenced by the inner retina. Additionally, melanopsin phototransduction has been linked to light-mediated changes in choroidal thickness (Sikka et al., 2014; Berkowitz et al., 2016). Though ORDs are less abundant in the mature retina, interactions between melanopsin ganglion cell ORDs and the vasculature remain uninvestigated.

We have found two morphologically distinct groups of melanopsin ganglion cell ORDs in the OPL are asymmetrically distributed to the dorsal retina. While this is a novel phenomenon in the mammalian retina, a ganglion cell to photoreceptor synapse is the rule rather than the exception in the invertebrate retina (Holmberg, 1970). Furthermore, ORDs in the OPL have recently been found in macaque tissue (Liao et al., 2016), suggesting the function of this potential circuit is important enough to persist evolutionarily. Even though the function remains to be elucidated, these morphological details are the first steps in resolving the function of these melanopsin ganglion cell outer retinal dendrites.

Acknowledgments

Acknowledgements of Support: NIH R15EY026255-01

We would like to thank Brittany Day for her technical services and Maureen Stabio for her invaluable advice on morphological analysis. We would also like to thank Dr. Qin Liu for generously allowing us to use his epifluorescence microscope. Use of the confocal was sponsored by the Department of Defense Office of Corrosion Policy and Oversight through the Engineering Research and Development Center/US Army Construction Engineering Research Laboratory Grant W9132T-11-0002 and we thank Daniel J. Dunmire and Richard Hays for their continued support.

LITERATURE CITED

Applebury ML, Antoch MP, Baxter LC, Chun LL, Falk JD, Farhangfar F, Kage K, Krzystolik MG, Lyass LA, Robbins JT. The murine cone photoreceptor: a single cone type expresses both S and M opsins with retinal spatial patterning. Neuron. 2000; 27(3):513–523. [PubMed: 11055434]

Baver SB, Pickard GE, Sollars PJ, Pickard GE. Two types of melanopsin retinal ganglion cell differentially innervate the hypothalamic suprachiasmatic nucleus and the olivary pretectal nucleus. The European journal of neuroscience. 2008; 27(7):1763–1770. [PubMed: 18371076]

Bellocchio EE, Hu H, Pohorille A, Chan J, Pickel VM, Edwards RH. The localization of the brain-specific inorganic phosphate transporter suggests a specific presynaptic role in glutamatergic transmission. J Neurosci. 1998; 18(21):8648–8659. [PubMed: 9786972]

Berkowitz BA, Schmidt T, Podolsky RH, Roberts R. Melanopsin Phototransduction Contributes to Light-Evoked Choroidal Expansion and Rod L-Type Calcium Channel Function In Vivo. Invest Ophthalmol Vis Sci. 2016; 57(13):5314–5319. [PubMed: 27727394]

Berson DM, Castrucci AM, Provencio I. Morphology and mosaics of melanopsin-expressing retinal ganglion cell types in mice. The Journal of comparative neurology. 2010; 518(13):2405–2422. [PubMed: 20503419]

Berson DM, Dunn FA, Takao M. Phototransduction by retinal ganglion cells that set the circadian clock. Science. 2002; 295(5557):1070–1073. [PubMed: 11834835]

Chew KS, Renna JM, McNeill DS, Fernandez DC, Keenan WT, Thomsen MB, Ecker JL, Loevinsohn GS, VanDunk C, Vicarel DC, Tufford A, Weng S, Gray PA, Cayouette M, Herzog ED, Zhao H, Berson DM, Hattar S. A subset of ipRGCs regulates both maturation of the circadian clock and segregation of retinogeniculate projections in mice. Elife. 2017 Jun.(6)

Dacey DM, Liao HW, Peterson BB, Robinson FR, Smith VC, Pokorny J, Yau KW, Gamlin PD. Melanopsin-expressing ganglion cells in primate retina signal colour and irradiance and project to the LGN. Nature. 2005; 433(7027):749–754. [PubMed: 15716953]

Ecker JL, Dumitrescu ON, Wong KY, Alam NM, Chen SK, LeGates T, Renna JM, Prusky GT, Berson DM, Hattar S. Melanopsin-expressing retinal ganglion-cell photoreceptors: cellular diversity and role in pattern vision. Neuron. 2010; 67(1):49–60. [PubMed: 20624591]

Estevez ME, Fogerson PM, Ilardi MC, Borghuis BG, Chan E, Weng S, Auferkorte ON, Demb JB, Berson DM. Form and function of the M4 cell, an intrinsically photosensitive retinal ganglion cell type contributing to geniculocortical vision. J Neurosci. 2012; 32(39):13608–13620. [PubMed: 23015450]

Fahrenkrug J, Nielsen HS, Hannibal J. Expression of melanopsin during development of the rat retina. Neuroreport. 2004; 15(5):781–784. [PubMed: 15073514]

Guler AD, Ecker JL, Lall GS, Haq S, Altimus CM, Liao HW, Barnard AR, Cahill H, Badea TC, Zhao H, Hankins MW, Berson DM, Lucas RJ, Yau KW, Hattar S. Melanopsin cells are the principal conduits for rod-cone input to non-image-forming vision. Nature. 2008; 453(7191):102–105. [PubMed: 18432195]

Hattar S, Liao HW, Takao M, Berson DM, Yau KW. Melanopsin-containing retinal ganglion cells: architecture, projections, and intrinsic photosensitivity. Science. 2002; 295(5557):1065–1070. [PubMed: 11834834]

Haverkamp S, Grunert U, Wassle H. The synaptic architecture of AMPA receptors at the cone pedicle of the primate retina. J Neurosci. 2001; 21(7):2488–2500. [PubMed: 11264323]

Holmberg K. The hagfish retina: fine structure of retinal cells in Myxine glutinosa, L., with special reference to receptor and epithelial cells. Zeitschrift fur Zellforschung und mikroskopische Anatomie. 1970; 111(4):519–538. [PubMed: 5485026]

Hoshi H, Liu WL, Massey SC, Mills SL. ON Inputs to the OFF Layer: Bipolar Cells That Break the Stratification Rules of the Retina. Journal of Neuroscience. 2009; 29(28):8875–8883. [PubMed: 19605625]

Hughes S, Watson TS, Foster RG, Peirson SN, Hankins MW. Nonuniform distribution and spectral tuning of photosensitive retinal ganglion cells of the mouse retina. Current biology: CB. 2013; 23(17):1696–1701. [PubMed: 23954426]

Johnson J, Tian N, Caywood MS, Reimer RJ, Edwards RH, Copenhagen DR. Vesicular neurotransmitter transporter expression in developing postnatal rodent retina: GABA and glycine precede glutamate. J Neurosci. 2003; 23(2):518–529. [PubMed: 12533612]

Kirkby LA, Feller MB. Intrinsically photosensitive ganglion cells contribute to plasticity in retinal wave circuits. Proceedings of the National Academy of Sciences of the United States of America. 2013; 110(29):12090–12095. [PubMed: 23821744]

Liao HW, Ren X, Peterson BB, Marshak DW, Yau KW, Gamlin PD, Dacey DM. Melanopsin-expressing ganglion cells on macaque and human retinas form two morphologically distinct populations. The Journal of comparative neurology. 2016; 524(14):2845–2872. [PubMed: 26972791]

Panda S, Sato TK, Castrucci AM, Rollag MD, DeGrip WJ, Hogenesch JB, Provencio I, Kay SA. Melanopsin (Opn4) requirement for normal light-induced circadian phase shifting. Science. 2002; 298(5601):2213–2216. [PubMed: 12481141]

Phillips MJ, Otteson DC, Sherry DM. Progression of neuronal and synaptic remodeling in the rd10 mouse model of retinitis pigmentosa. The Journal of comparative neurology. 2010; 518(11):2071–2089. [PubMed: 20394059]

Provencio I, Jiang G, De Grip WJ, Hayes WP, Rollag MD. Melanopsin: An opsin in melanophores, brain, and eye. Proc Natl Acad Sci U S A. 1998; 95(1):340–345. [PubMed: 9419377]

Provencio I, Rodriguez IR, Jiang GS, Hayes WP, Moreira EF, Rollag MD. A novel human opsin in the inner retina. Journal of Neuroscience. 2000; 20(2):600–605. [PubMed: 10632589]

Renna JM, Chellappa DK, Ross CL, Stabio ME, Berson DM. Melanopsin ganglion cells extend dendrites into the outer retina during early postnatal development. Developmental neurobiology. 2015; 75(9):935–946. [PubMed: 25534911]

Renna JM, Weng S, Berson DM. Light acts through melanopsin to alter retinal waves and segregation of retinogeniculate afferents. Nature neuroscience. 2011; 14(7):827–829. [PubMed: 21642974]

Schiviz AN, Ruf T, Kuebber-Heiss A, Schubert C, Ahnelt PK. Retinal cone topography of artiodactyl mammals: influence of body height and habitat. The Journal of comparative neurology. 2008; 507(3):1336–1350. [PubMed: 18189305]

Schleich CE, Vielma A, Glosmann M, Palacios AG, Peichl L. Retinal photoreceptors of two subterranean tuco-tuco species (Rodentia, Ctenomys): morphology, topography, and spectral sensitivity. The Journal of comparative neurology. 2010; 518(19):4001–4015. [PubMed: 20737597]

Schmidt TM, Chen SK, Hattar S. Intrinsically photosensitive retinal ganglion cells: many subtypes, diverse functions. Trends in neurosciences. 2011; 34(11):572–580. [PubMed: 21816493]

Schmidt TM, Kofuji P. Structure and function of bistratified intrinsically photosensitive retinal ganglion cells in the mouse. The Journal of comparative neurology. 2011; 519(8):1492–1504. [PubMed: 21452206]

Schmidt TM, Taniguchi K, Kofuji P. Intrinsic and extrinsic light responses in melanopsin-expressing ganglion cells during mouse development. Journal of neurophysiology. 2008; 100(1):371–384. [PubMed: 18480363]

Sekaran S, Lupi D, Jones SL, Sheely CJ, Hattar S, Yau KW, Lucas RJ, Foster RG, Hankins MW. Melanopsin-dependent photoreception provides earliest light detection in the mammalian retina. Current biology: CB. 2005; 15(12):1099–1107. [PubMed: 15964274]

Sherry DM, Wang MM, Bates J, Frishman LJ. Expression of vesicular glutamate transporter 1 in the mouse retina reveals temporal ordering in development of rod vs. cone and ON vs. OFF circuits. The Journal of comparative neurology. 2003; 465(4):480–498. [PubMed: 12975811]

Sikka G, Hussmann GP, Pandey D, Cao S, Hori D, Park JT, Steppan J, Kim JH, Barodka V, Myers AC, Santhanam L, Nyhan D, Halushka MK, Koehler RC, Snyder SH, Shimoda LA, Berkowitz DE.

Melanopsin mediates light-dependent relaxation in blood vessels. Proceedings of the National Academy of Sciences of the United States of America. 2014; 111(50):17977–17982. [PubMed: 25404319]

Szel A, Lukats A, Fekete T, Szepessy Z, Rohlich P. Photoreceptor distribution in the retinas of subprimate mammals. Journal of the Optical Society of America A, Optics, image science, and vision. 2000; 17(3):568–579.

Valiente-Soriano FJ, Garcia-Ayuso D, Ortin-Martinez A, Jimenez-Lopez M, Galindo-Romero C, Villegas-Perez MP, Agudo-Barriuso M, Vugler AA, Vidal-Sanz M. Distribution of melanopsin positive neurons in pigmented and albino mice: evidence for melanopsin interneurons in the mouse retina. Frontiers in neuroanatomy. 2014; 8:131. [PubMed: 25477787]

Vugler AA, Redgrave P, Semo M, Lawrence J, Greenwood J, Coffey PJ. Dopamine neurones form a discrete plexus with melanopsin cells in normal and degenerating retina. Exp Neurol. 2007; 205(1):26–35. [PubMed: 17362933]

Zhang DQ, Wong KY, Sollars PJ, Berson DM, Pickard GE, McMahon DG. Intraretinal signaling by ganglion cell photoreceptors to dopaminergic amacrine neurons. Proceedings of the National Academy of Sciences of the United States of America. 2008; 105(37):14181–14186. [PubMed: 18779590]

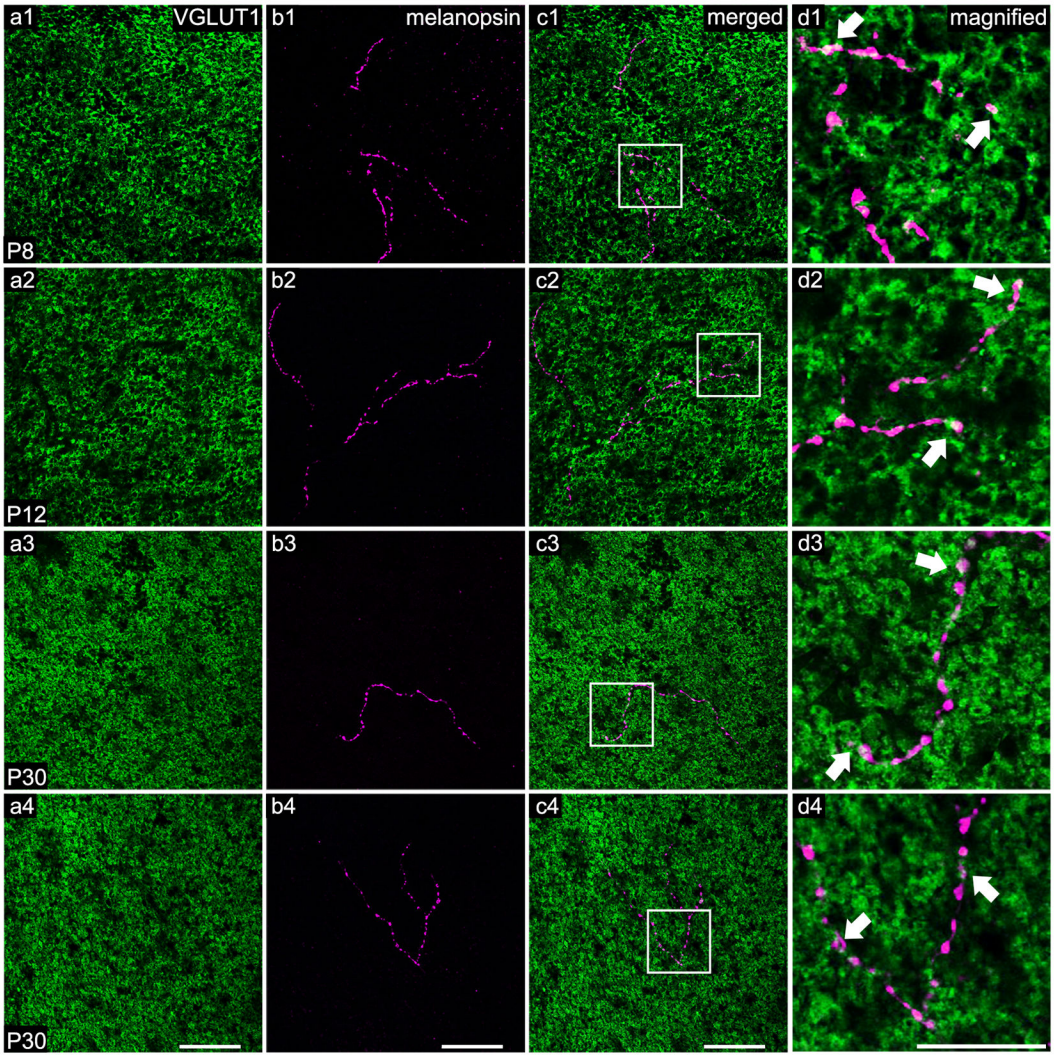

Figure 1. ORDs stratify in the OPL and lie closely opposed to cone photoreceptor terminals at all developmental ages and in the adult

A single optical section (0.45 μm) generated from a series of confocal images masked to correct for the imperfect flatness of the retina. Immuno-positive photoreceptor terminals (VGLUT1) are labeled in green and melanopsin ORDs stratifying in the OPL are labeled in magenta. White areas (indicated with arrows) suggest regions of overlap between melanopsin staining and VGLUT1 staining. a1–d1) A branched ORD from a M1 melanopsin ganglion cell at P8. a2–d2) A branched ORD from a displaced M1 melanopsin ganglion cell at P12. a3–d3) An unbranched ORD from a M1 melanopsin ganglion cell at P30 (adult). a4–d4) A branched ORD from a displaced melanopsin ganglion cell at P30 (adult). Scale bar: 50 μm; Magnified scale bar: 25 μm.

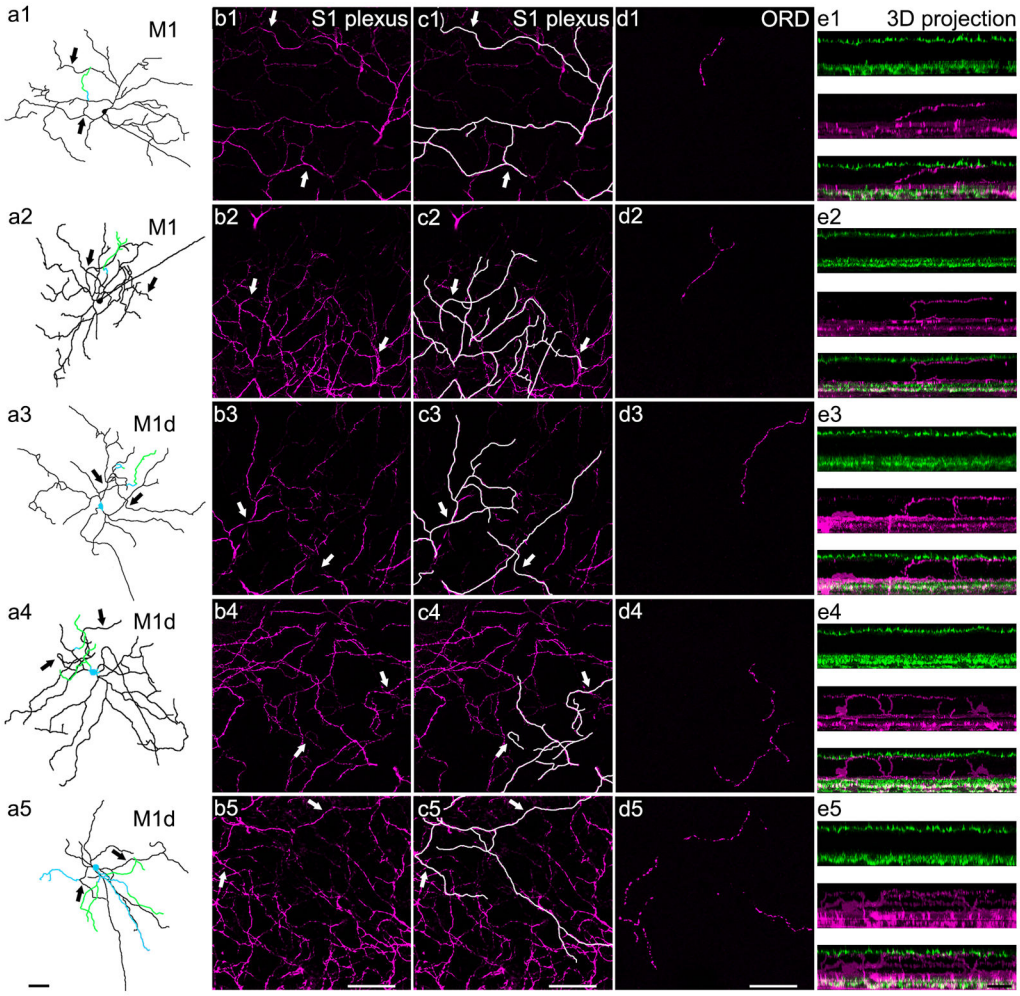

Figure 2. ORDs in the OPL originate from a subset of biplexiform M1 and M1d melanopsin ganglion cells and exhibit five general dendritic morphologies

a1–a5) Whole cell reconstructions of biplexiform melanopsin ganglion cells with each type of ORD morphology at P12. Images are depth-coded so that black represents dendrites or somas in the GCL and IPL, blue represents dendrites or somas in the INL, and green represents dendrites that stratify in the OPL. Both M1 and M1d cells are known to have dendrites that stratify in the S1 plexus, so arrows indicate dendrites that can be seen in both the whole cell tracings and the confocal images of the S1 plexus to the right. From top to bottom: M1 with an unbranched ORD, M1 with a branched ORD, M1d with an unbranched ORD, M1d with a branched ORD, and M1d with an ORD in the OPL as well as an ORD in the INL. b1–b5) Confocal optical sections (0.50 μm) of the melanopsin-immunopositive S1 plexus (magenta). Arrows indicate dendrites in the S1 plexus that can also be seen in the respective whole cell tracings in the first column. c1–c5) Confocal optical sections (0.50 μm) of the melanopsin-immunopositive S1 plexus (magenta). Dendrites that are present in both the whole cell tracing and the S1 plexus have been highlighted for clarity. Arrows indicate dendrites in the S1 plexus that can also be seen in their respective whole cell tracings in the first column. d1–d5) A single optical section (0.50 μm) generated from a series of confocal images masked to correct for the imperfect flatness of the retina. Immunopositive

melanopsin ORDs stratifying in the OPL (magenta). e1–e5) 3D projections of confocal z-stacks (magenta=melanopsin, green=VGLUT1) to show the 21 biplexiform nature of a subset of M1 and M1d melanopsin ganglion cells. a1–d5 scale bars: 50 μm; e1–e5 scale bar: 25 μm.

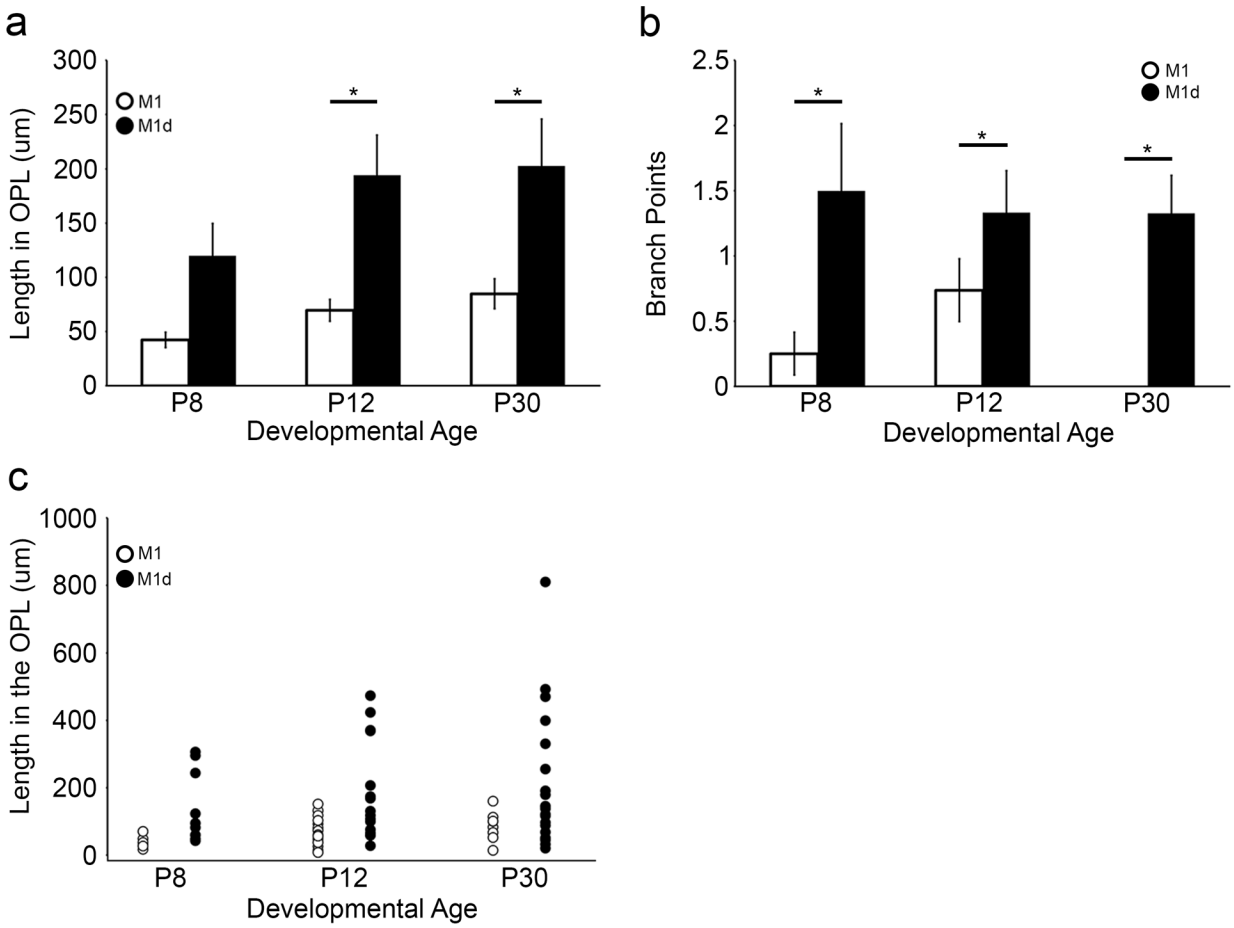

Figure 3. Melanopsin ganglion cell ORDs in the OPL form two morphologically distinct groups

a) ORDs in the OPL that originate from M1 cells are significantly shorter than those that originate from M1d cells at P12 and P30 (n=5 retinas at each developmental age; $p<0.05$). b) ORDs in the OPL that originate from M1 cells have fewer branch points than those that originate from M1d cells (n=5 retinas at each developmental age; $p<0.05$). From these results, it appears that the greater length of M1d ORDs within the OPL is due to greater number of branch points. c) A scatter plot of ORD length in the OPL at different developmental time points. ORDs in the OPL from M1 cells have less dendrite in the OPL than those of M1d cells. ORDs that are longer (approximately >200 μm) have more than two branch points. Thus, the greater total length of M1 ORDs in the OPL seems to be due to a greater number of branch points. Error bars=SEM.

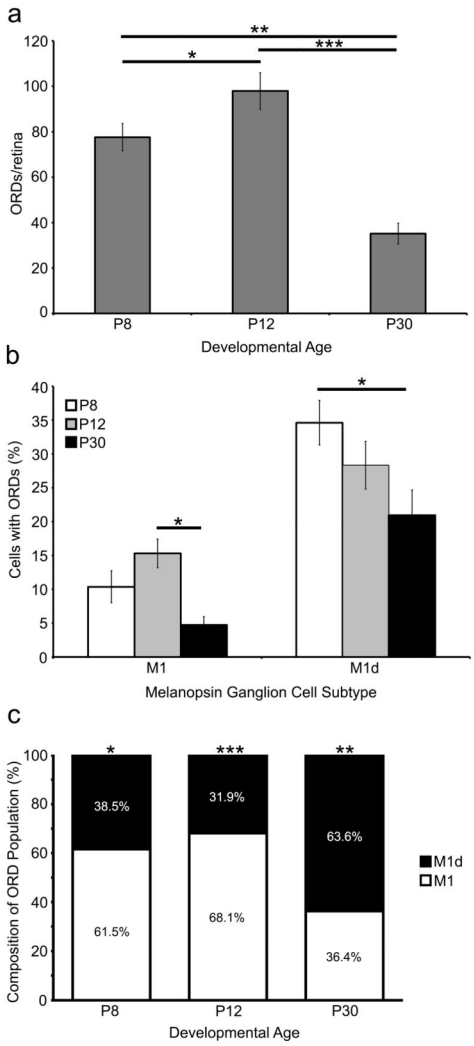

Figure 4. A subset of M1 and M1d melanopsin ganglion cells have ORDs in the INL and OPL during development and in the adult mouse retina

a) The number of ORDs in the OPL and the INL changes throughout development. The number of ORDs increases from P8 to P12 ($p<0.05$) and then decreases from P12 to P30 ($p<0.001$). b) The percentage of M1 and M1d cells in the retina that have ORDs in the OPL and/or INL during development and in the adult. Unsurprisingly, the highest number of ORD-positive M1 and M1d cells is during development. The number of ORD-positive M1 cells decreases significantly from P12 to P30 ($p<0.05$), and the number of ORD-positive M1d cells decreases significantly from P8 to P30 ($p<0.05$). c) The percentage of ORDs in the OPL and INL that originate from M1 cells compared to those that originate from M1d cells. At P8 and P12, the majority of ORDs originate from M1 melanopsin ganglion cells ($p<0.05$ and $p<0.001$, respectively). However, at P30, the majority of ORDs originate from M1d melanopsin ganglion cells ($p<0.01$). Error bars=SEM.

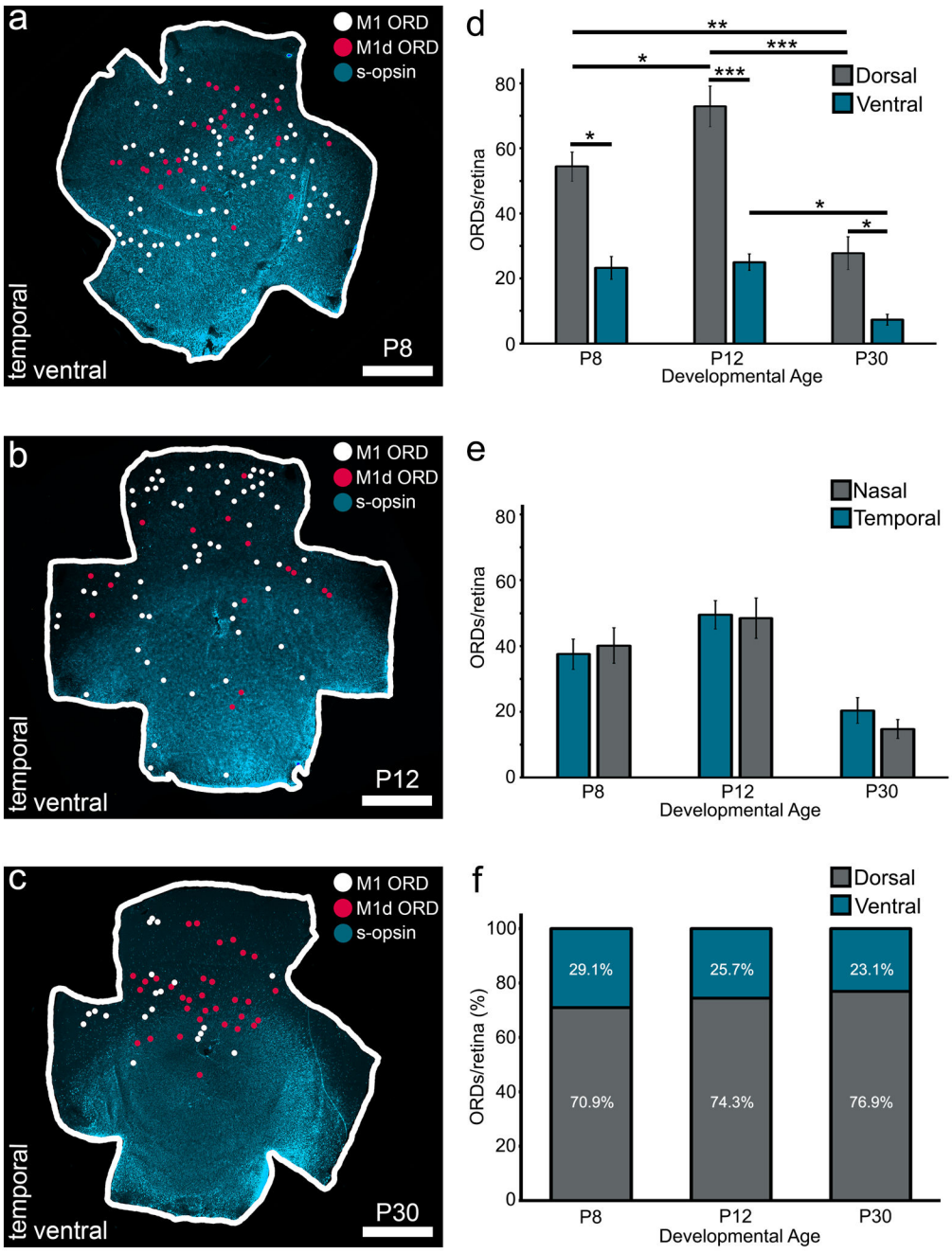

Figure 5. ORDs are asymmetrically distributed to the dorsal retina at all developmental timepoints

a–c) Wholemount retinas with s-opsin immunohistochemistry (blue), M1 ORD locations (white circles), and M1d ORD locations (pink circles). From left to right: P8 retina (a), P12 retina (b), P30 (c) retina. Scale bar: 1mm. d) ORDs are asymmetrically distributed to the dorsal retina as early as P8 (P8 retinas n=7; P12 retinas n=11; P30 retinas n=8; P8 dorsal vs. ventral: $p<0.05$; P12 dorsal vs. ventral: $p<0.001$; P30 dorsal vs. ventral: $p<0.05$). The amount of dorsal ORDs increases from P8 to P12 ($p<0.05$), P8 to P30 ($p<0.01$) and decreases from P12 to P30 ($p<0.001$). The amount of ventral ORDs does not change

significantly across development ($p>0.05$) except for a slight decrease between P12 and P30 ($p<0.05$).e) ORDs are evenly distributed across the nasal and temporal retina at all developmental time points ($p>0.05$). F) The proportion of ORDs in the dorsal retina when compared to the proportion of ventral ORDs does not change across development ($p>0.05$). Error bars=SEM.

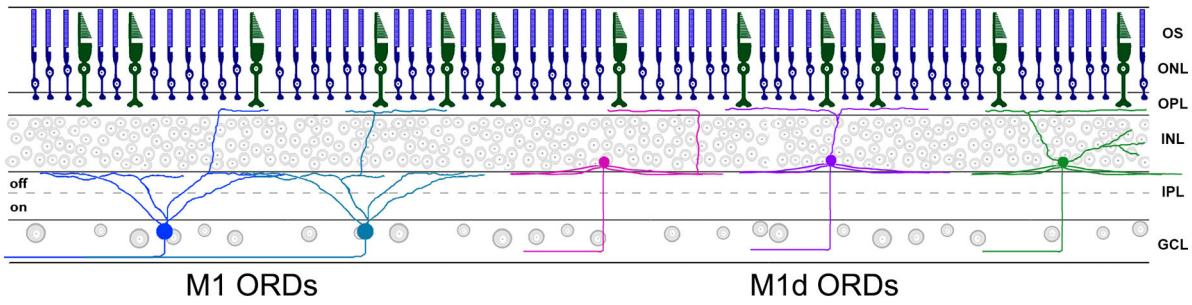

Figure 6.

A retinal schematic of each type of ORD in the OPL as found in the mouse retina. ORDs from M1 cells originate from dendrites within the OFF sublamina of the IPL, extending through the INL to run briefly along the OPL. ORDs from M1d cells originate either at the soma or at dendrites in the S1 plexus to extend straight up through the INL and stratify extensively within the OPL. ORDs in the OPL from both subtypes lie in close proximity to cone photoreceptor terminals. From left to right: M1 with unbranched ORD, M1 with branched ORD, M1d with unbranched ORD, M1d with branched ORD, M1d with ORDs in both the INL and OPL.

Table 1

Primary Antibodies

Name	Structure of Immunogen	Manufacturer	Concentration
Rabbit-anti-Melanopsin	15 most N-terminal amino acids of mouse melanopsin extracellular domain (MDSPSGPRVLSSLTQC)	Advanced Targeting Systems San Diego, CA Cat#: AB-38 (UF006) RRID: AB_2314781 Host: Rabbit Polyclonal	1:10,000
Guinea pig anti-VGLUT1	Synthetic peptide from rat VGLUT1 protein (GATHSTVQPPRPPPPVRDY)	EMD Millipore Billerica, MA Cat#: AB5905 RRID: AB_2301751 Host: Guinea pig Polyclonal	1:1000
DAPI	AT regions of dsDNA	Thermofisher Scientific Waltham, MA Cat#: D1306 RRID: AB_2629482	1:200
DRAQ5	DNA; nuclear stain	Thermofisher Scientific Waltham, MA Cat#: 62252	1:200
Goat anti-S-opsin	N- terminus of human OPN1SW protein (EFYLFKNISSVGPWDGPQYH)	Santa Cruz Biotechnology Dallas, TX Cat#: sc14363 RRID: AB_2158332 Host: Goat Polyclonal	1:500

Table 2

ORDs in the OPL from M1d cells are longer than ORDs from M1 cells

Age	M1	M1d
P8	42.27 ± 7.03 μm	119.98 ± 29.49 μm
P12	69.54 ± 9.97 μm	194.11 ± 36.89 μm
P30	84.81 ± 13.74 μm	202.69 ± 43.17 μm

Table 3

ORDs in the OPL from M1d cells have more branch points than ORDs from M1 cells

Age	M1	M1d
P8	0.25 ± 0.16	1.5 ± 0.51
P12	0.74 ± 0.24	1.33 ± 0.32
P30	0	0.81 ± 0.29

Table 4

Cell counts and number of ORD-positive cells in the retina throughout development

Age	M1 Cells	ORD$^+$ M1 cells	M1d cells	ORD$^+$ M1d cells
P8	212	39	57	15
	264	25	65	20
	241	16	55	24
	270	19	53	20
P12	298	44	78	25
	299	29	57	20
	352	61	74	14
	256	50	66	18
P30	283	13	70	22
	263	9	71	10
	254	21	73	15
	190	5	51	9

Table 5

Abbreviations used in figure legends

ORDs	outer retinal dendrites
M1	M1 subtype of melanopsin ganglion cells
M1d	displaced M1 subtype of melanopsin ganglion cells
OS	outer segment
ONL	outer nuclear layer
OPL	outer plexiform layer
INL	inner nuclear layer
IPL	inner plexiform layer
GCL	ganglion cell layer
P8	postnatal day 8
P12	postnatal day 12
P30	postnatal day 30